A major purpose of the Technical Information Center is to provide the broadest dissemination possible of information contained in DOE's Research and Development Reports to business, industry, the academic community, and federal, state and local governments.

Although a small portion of this report is not reproducible, it is being made available to expedite the availability of information on the research discussed herein.

LA-UR -83-2589

CONF-8308104--15

Los Alamos National Laboratory is operated by the University of California for the United States Department of Energy under contract W-7405-ENG-36

LA-UR--83-2589

DE84 001358

TITLE SHALLOW LAND BURIAL TECHNOLOGY -- ARID

AUTHOR(S) W. V. Abeele, G. L. DePoorter, T. E. Hakonson, and J. W. Nyhan

SUBMITTED TO Fifth Annual DOE LLWP Participants Information Meeting, Denver, CO, August 30, 1983.

DISCLAIMER

MASTER

Los Alamos Los Alamos National Laboratory
Los Alamos, New Mexico 87545

SHALLOW LAND BURIAL TECHNOLOGY—ARID

W. V. Abeele, G. L. DePoorter, T. E. Hakonson, and J. W. Nyhan
Los Alamos National Laboratory

ABSTRACT

Scope of the tasks being performed by Los Alamos will be identified. Emphasis will be placed upon the geotechnical work. Important geotechnical properties of a low level waste disposal site include hydraulic conductivity, consolidation, and shear strength of the applicable medium. The hydraulic conductivity of crushed Bandelier tuff has been assessed using the instantaneous profile method. The best fit of hydraulic conductivity as a function of water content was found to be a power function. The coefficient of consolidation was difficult to measure because of the relatively high hydraulic conductivity. The repose angle for crushed tuff is higher than the normally expected range. This is probably because of a higher than average angularity and surface roughness. The high coefficient of consolidation and high internal friction angle make finely crushed tuff a material with ideal mechanical characteristics. The drawback is that a high coefficient of consolidation is linked to a high hydraulic conductivity.

INTRODUCTION

Determining the potential impact of buried radioactive wastes on the environment requires definition of the mechanisms and rates by which the radionuclides can enter the environment. The various mechanisms can be divided into two major categories--natural phenomena more or less independent of human activity, and advertent acts by man, such as war, land excavation, sabotage, etc. All natural processes can be further subdivided into two groups: chronic release processes, which occur at a more or less uniform rate when viewed on a time scale of tens to hundreds of years, and acute release processes consisting of single events separated by long periods of nonoccurrence. Chronic release mechanisms include subsurface transport of radionuclides by migrating water.[1] Hydraulic conductivity, the main control for subsurface transport of radionuclides, is most important for assessment of containment capabilities.

Knowledge of consolidation and shear strength of backfill, used as interlayers and cap in waste pits, will help in the evaluation of the subsidence potential. Failure of *any* engineering structure may indeed occur in one of two ways: excessive settlement or shear failure of the supporting soil.

The engineering structures involved may include entire cities (e.g., Mexico City), building complexes, or parts of buildings. Partial building subsidence is caused mainly by uneven soil settlements. The best known example of this is the leaning tower of Pisa, which is only famous because it has not fallen down in 8 centuries despite its still settling foundations. Natural or anthropogenic modification of the landscape may also be subject to failures (e.g., slopes, modification of supporting medium in landfills). Differential settlements are usually structurally the most critical.

Of the three phases possibly present in soil, only the solid phase controls the resistance to compression and shear. Water, present in a moist soil, is highly incompressible but, as a liquid, is by definition not capable of resisting shear loads. Air, present in unsaturated soils, will not support compression or shear loads.

In a saturated soil, compression will be caused mainly by expulsion of water out of the soil voids. Under the influence of an externally applied load, the expulsion of water from the voids is highly dependent on the permeability of the medium. The extremely low permeability in the case of clay leads to a slow void contraction. The compression of saturated, low permeability layers under a static pressure is known as consolidation. The consolidation rate depends on the compressibility of the soil (rate of decrease in volume with stress) and soil permeability, which, in turn, is dependent on the viscosity of the liquid (viscosity of water at 35°C is half that at 5°C). An increase in temperature increases the consolidation *rate* but does not affect *total* amount of consolidation.[2]

The oedometer test maintains a constant stress until settlement is virtually complete and no evidence of neutral stress or pore pressure remains. Initially, the stress is converted into increased pore pressure. As water is expelled out of the soil voids, the pore pressure gradually drops off to zero. The results are read as a plot of void ratio vs time for a given total stress (neutral + effective).

Failure to drain the pores will result in low shear resistance. The ability to resist shear loads is solely dependent on the mechanical interaction of the solid particles in the soil matrix. The presence of excess water reduces the effective stress responsible for the friction between solids.

BIOINTRUSION BARRIER TESTING

Results from small scale lysimeters to evaluate the effectiveness of several geologic materials as plant root and burrowing animal intrusion barriers[1,2] led to the selection of cobble (7-13 cm diameter) overlain by gravel (<2 cm diameter) as the most effective intrusion barrier tested. Additional experiments were undertaken with rock intrusion barriers to evaluate:

- performance with time,
- effectiveness at intermediate and field scale,
- the effect on water percolation in order to estimate optimum top soil depth, and
- the effect of various degrees of subsidence on the intrusion barrier integrity.

Those experiments will not be discussed in this paper.

CAPILLARY BARRIER FIELD TESTING

Small scale modeling has demonstrated that it was possible to maintain structures dry in porous media by using capillary barriers. These barriers are created by differences in particle size distribution. The phenomenon is due to the predominance of capillary suction, soil tension, or matric potential over gravity forces. The percolating liquid will only penetrate the coarser material after the overlying finer one is totally wetted. Consequently, the structure enclosed in the coarser material is maintained dry. As long as the matric potential at the coarse/fine interface remains negative, water infiltrating into the finer layer will not cross the interface but will flow laterally within the finer layer until percolation recurs upon reaching the edge of the coarser layer. This concept has been referred to as the "wick effect." The lateral distance over which the water can be transported is limited and will be influenced by the slope of the interface.

The experimental configuration is illustrated in Fig. 1. The materials used in both experiments were crushed Bandelier tuff and gravel. Capillary barrier performance is directly proportional to the sharpness of the particle size difference at the interface. The slope of the interface was set at 15% in one experiment and at 0% in the control experiment.

Figure 2 is a summary of the experimental results for the configuration with the 15% slope. Higher moisture contents and time lags in the crests of downslope points show that the wick system basically works.

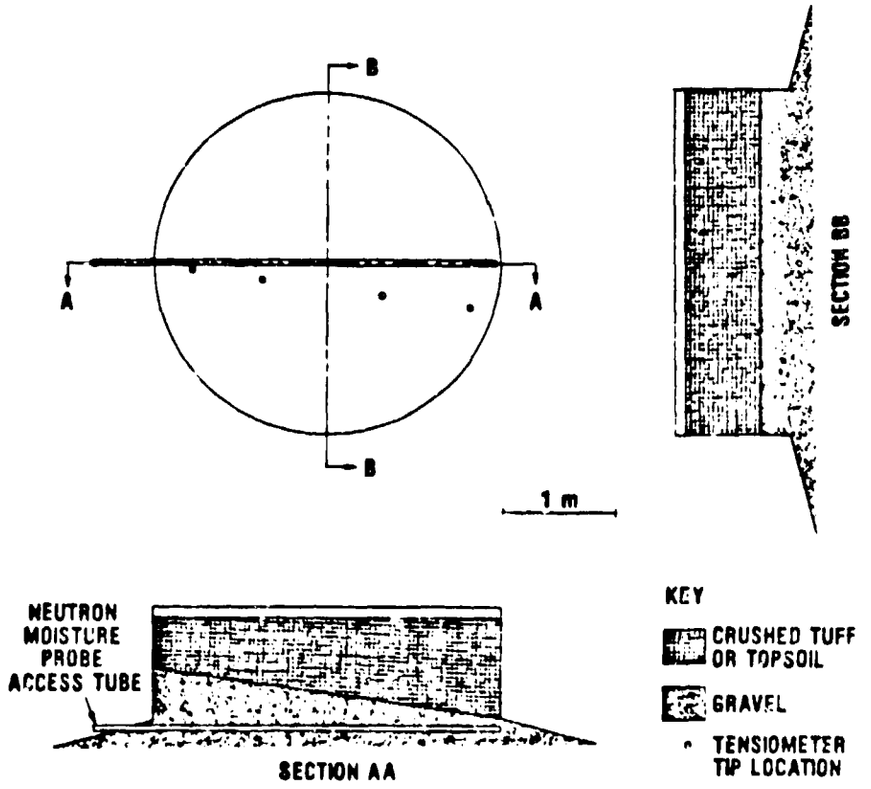

Fig. 1. Wick experiment.

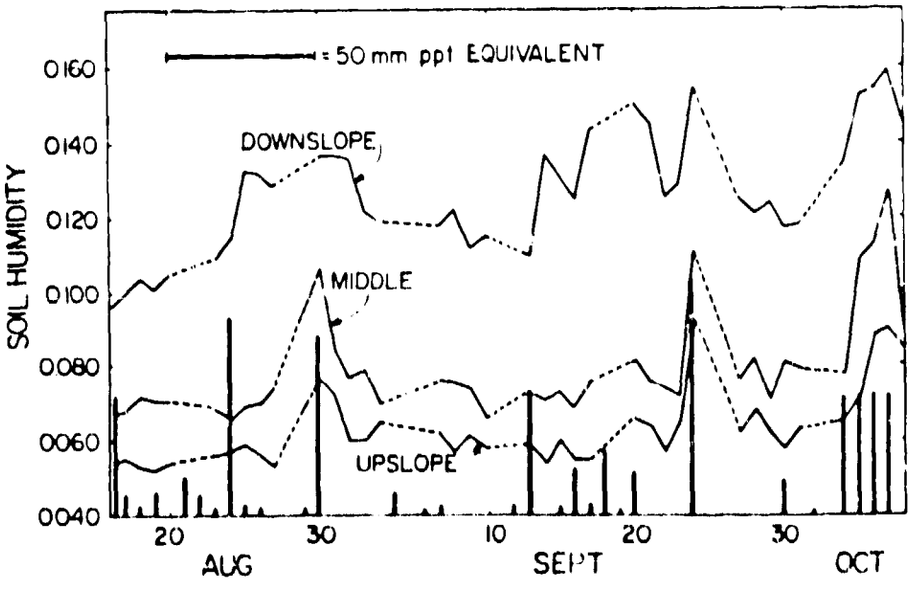

Fig. 2. Integrated moisture content (soil humidity) as a function of ppt equivalent.

HYDRAULIC CONDUCTIVITY

The soil column used for measurement of saturated and unsaturated hydraulic conductivity is 3 m in diameter and 6 m deep with access ports along the entire height of the profile and a drain at the bottom. The column was filled with crushed Bandelier tuff, which consists mostly of silicic glass and has a grain size distribution close to that of a silty sand. At the bottom of the experimental unit the drain was covered with a coarse screen. Approximately 0.25 m of gravel as placed over the screen and above this was placed approximately 0.25 m of sand. The rest of the column profile was crushed Bandelier tuff, which was obtained locally.

After crushing, the tuff was screened at a cement batch plant. All material passing through a 12.5 mm screen was mixed with known amounts of water to give optimum water content for compaction, thus ensuring column uniformity and minimal subsidence. Water content and wet and dry density were measured at several heights during the filling operation. At each 0.2 m thick increment, the tuff was compacted by use of tampers. Independent studies done at Los Alamos[1] showed that the optimal tuff wetness for compaction was 12% by mass. The amount of moisture present, between 10 and 13% by mass, is close to this optimum amount. Dry density obtained varied with depth from 91.3 to 101.4% of what is considered optimum dry density for crushed tuff. Maximum compaction was not obtained at some of the lower depths, where the moisture content was occasionally too high.

Tensiometers were inserted with a downward slope of 13% to the horizontal. They were inserted 196.5 mm above the horizontal neutron probe access tubes so that the cup of the tensiometer would be at the same height as the access tube. Also, the tensiometer cup was at an average horizontal distance of 0.44 m from the access tube and therefore well outside the radius of influence of the neutron probe.[3]

The column was flooded and allowed to saturate by ponding a layer of water about 50 mm thick on the surface. Finally, the surface was covered to prevent any further water flux into the soil column from rainfall or out of the column by evaporation. The column was then allowed to drain for 100 days. The volumetric outflow rate of water at the drain was measured regularly during flooding and drainage.

The experiment was maintained in a flooded condition for almost a month. During this time, the saturation level increased gradually and finally leveled out at an average volumetric water content, θ_v, of 0.331 (standard deviation 0.013) and a maximum saturation level of 0.346. These fluctuations in saturation level may be partly caused by some layering or stratification. This layering effect, however, should not in any way interfere with the validity of the method.[4]

The results of the measurements are shown in Figs. 3 through 6. Figure 3 is a plot of volumetric outflow rate as a function of time for the entire 100 days of the experiment. Figure 4 is a plot of volumetric water content as a function of depth for selected days during the drainage starting with saturation at day zero. Figure 5 is a plot of matric potential as a function of depth for selected days during the drainage. Figure 6 is the soil moisture characteristic curve obtained from the simultaneous measurement of volumetric water content and

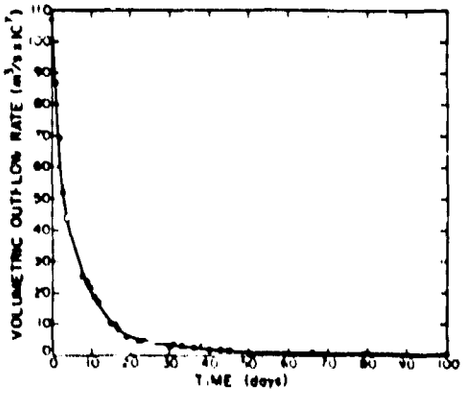

Fig. 3 Measured volumetric outflow rate.

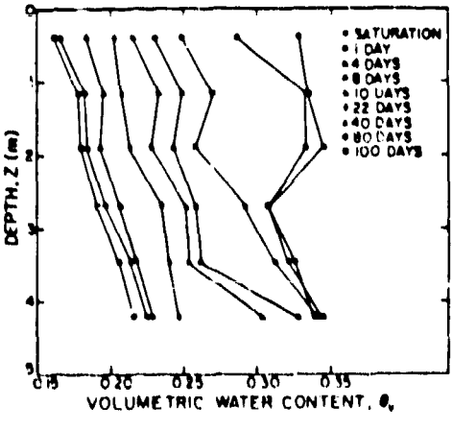

Fig. 4. Measured volumetric water content as a function of depth for selected times.

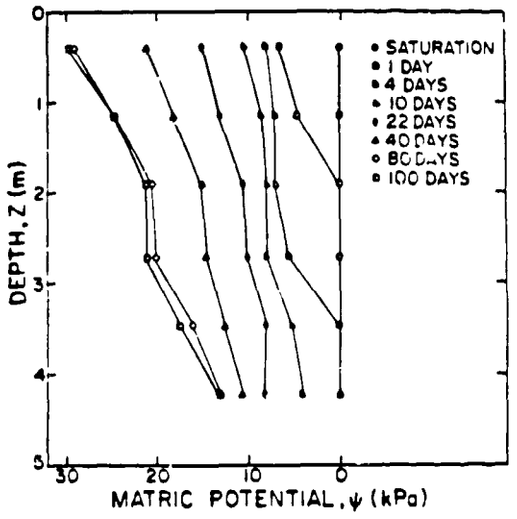

Fig. 5. Measured matric potential as a function of depth for selected times.

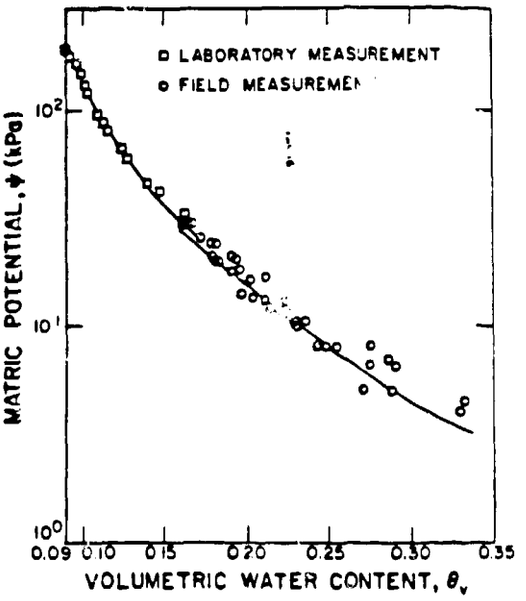

Fig. 6. Soil moisture characteristic curve from both laboratory and field measurements. The drawn curves are best fit curves from regression analysis.

matric potential. This equation is valid for the volumetric water content range from 0.16 to 0.33. For the lower moisture contents, the values reported by Abeele[5] are shown in Fig. 6. With the experimental results just presented, both the saturated and unsaturated hydraulic conductivities can be calculated.

The unsaturated hydraulic conductivity as a function of water content was determined by the instantaneous profile method of Watson.[6] The calculation procedure described by Hillel et al.[4] was used in this paper. This method requires the simultaneous measurement of the matric potential of the soil by tensiometers as a function of time and depth and measurement of the soil volumetric water content as the same function of time and depth in the soil profile by means of a neutron moisture probe. From these data, the unsaturated hydraulic conductivity can be calculated as a function of water content. The mathematical description of the instantaneous profile method can be found in the aforementioned references.

The hydraulic conductivity is the ratio of the flux to the total hydraulic head gradient (gravitational plus matric). To calculate the flux, the derivative of the volumetric water content/time curve is required. To calculate this derivative, a plot is made of volumetric water content against time for each of the depths at which measurements were made. The data for depths of 0.40, 2.71, and 4.23 m are shown in Fig. 7. The data and curves for the other three depths are similar. A best fit curve was obtained for each depth by regression analysis. The equation and best fit parameters for each depth are given in Table 1. From these equations, the volumetric water content and time derivative of the volumetric water content can be calculated for any time. For these calculations, times of 1, 4, 10, 20, 40, 80, and 100 days were chosen (column 1 of Table 2). Measurements of water content and matric potential were made at depths of 0.4, 1.16, 1.91, 2.71, 3.47, and 4.23 m from the surface (z_{tot} in column 4 of Table 2). Based on this spacing, the column was divided into zones for calculational purposes. The boundary between the zones is taken as halfway between the locations at which the measurements were made. The zone boundaries and zone thickness, dz, are given in columns 2 and 3, respectively, of Table 2. The volumetric water content, θ_v, and time derivative of the volumetric water content, $\partial\theta/\partial t$, were calculated at each depth for every time and the values entered into columns 5 and 6, respectively, of Table 2.

The rate of volumetric water content change in each layer, $dz(\partial\theta/\partial t)$, is calculated by multiplying the derivative of the water content/time curve by its respective depth increment. These values are given in column

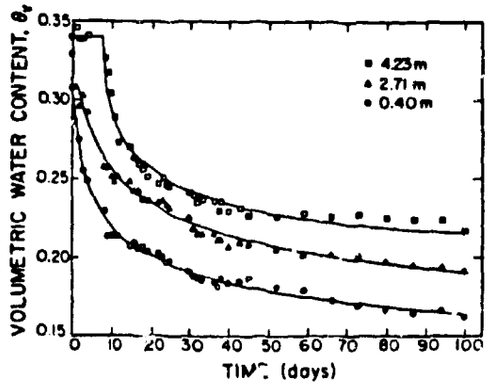

Fig. 7. Volumetric water content as a function of time at three selected depths.

TABLE 1

BEST FIT CURVES FOR VOLUMETRIC WATER CONTENT DATA

Depth (m)	Equation	r^2
0.40	$\theta_v = 0.293\ d^{-0.126}$	0.99
1.16	$\theta_v = 0.312\ d^{-0.125}$	0.96
1.91	$\theta_v = 0.319\ d^{-0.128}$	0.95
2.71	$\theta_v = 0.344\ d^{-0.129}$	0.98
3.47	$\theta_v = 0.317\ d^{-0.094}$	0.97
4.23	$\theta_v = 0.323\ (d-7)^{-0.091}$	0.96

7 of Table 2 in units of m day^{-1}. The flux through each layer, q, is calculated by summing the rates of change in water content for all the layers from the layer of interest to the top of the experiment. These values are given in column 8 of Table 2 and are again in units of m day^{-1}. The flux is one of the quantities required to calculate the hydraulic conductivity as a function of water content.

The other quantity required is the hydraulic head gradient. This is obtained by adding the gravitational to the matric potential at each elevation, plotting against depth, and determining the slope by regression analysis. Matric potential was plotted against time for the measurements at each depth. Plots for depths of 0.40, 2.71, and 4.23 m are shown in Fig. 8. The data for the other three curves are similar. Best fit curves were obtained for each set of data by regression analysis. The equations and best fit parameters are given in Table 3. Using these best fit equations, matric potentials, ψ, were calculated at each of the times in column 1 of Table 2 and included in column 9 of this table. The total hydraulic head, H, was calculated and is listed in column 10 of Table 2.

Division of the flux by the corresponding hydraulic gradient yields the hydraulic conductivity in m day^{-1}. These data are all plotted in Fig. 9, including the value at saturation (1.44×10^{-6} m s^{-1}). The hydraulic conductivity can now be calculated as a function of water content by volume. In this case, the best fit was a power function of the water content by volume, which will be a straight line when plotted on a log-log graph. The equation is $K = 0.0108\ \theta_v^{8.33}$, with an r^2 of 0.96. The extrapolated curve from the laboratory measurements of Abeele[5] is also shown in Fig. 9.

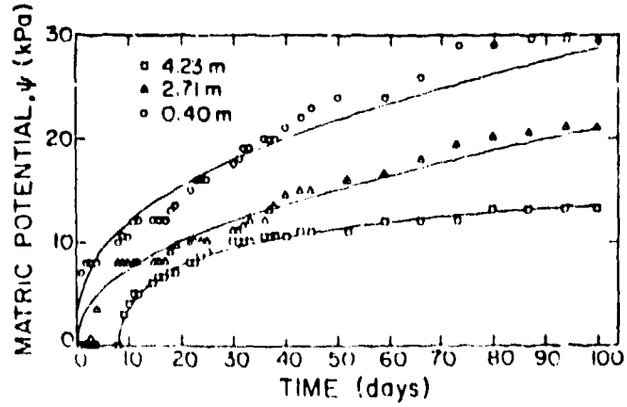

Fig. 8 Matric potential as a function of time at three selected depths.

TABLE 2

CALCULATION OF HYDRAULIC CONDUCTIVITY AFTER 100 DAYS

t	Layer Boundaries (m)	dz (m)	Z_{tot} (m)	θ_s	$-\partial\theta/\partial t$ (day^{-1})	$-dz(\partial\theta/\partial t)$ (m day^{-1})	q (m day^{-1})	$-\psi$ (m)	H (m)	$\partial H/\partial Z_{tot}$	K × 10^{-6} (m/s)
1	0 - 0.78	0.78	0.40	0.29345	0.03709	0.02893	0.02893	0.51	0.91	0.86749	38.60
	0.78 - 1.54	0.76	1.16	0.31176	0.03912	0.02973	0.05866	0.39	1.55		78.26
	1.54 - 2.31	0.77	1.91	0.31889	0.04093	0.03152	0.09018	0.31	2.22		120.32
	2.31 - 3.09	0.78	2.71	SAT.							
	3.09 - 3.85	0.76	3.47								
	3.85 - 4.61	0.76	4.23								
4	0 - 0.78	0.78	0.40	0.24628	0.00778	0.00607	0.00607	0.85	1.25	0.84288	8.335
	0.78 - 1.54	0.76	1.16	0.26198	0.00822	0.00625	0.01232	0.68	1.84		16.92
	1.54 - 2.31	0.77	1.91	0.26691	0.00856	0.00659	0.01891	0.55	2.46		25.97
	2.31 - 3.09	0.78	2.71	0.28739	0.00926	0.00722	0.02613	0.49	3.20		35.88
	3.09 - 3.85	0.76	3.47	SAT.							
	3.85 - 4.61	0.76	4.23								
10	0 - 0.78	0.78	0.40	0.21935	0.00277	0.00216	0.00216	1.20	1.60	0.79260	3.16
	0.78 - 1.54	0.76	1.16	0.23352	0.00293	0.00223	0.00439	0.98	2.14		6.41
	1.54 - 2.31	0.77	1.91	0.23730	0.00305	0.00235	0.00674	0.80	2.71		9.83
	2.31 - 3.09	0.78	2.71	0.25538	0.00329	0.00257	0.00931	0.74	3.45		13.60
	3.09 - 3.85	0.76	3.47	0.25538	0.00239	0.00182	0.01113	0.54	4.01		16.25
	3.85 - 4.61	0.76	4.23	0.29249	0.00240	0.00182	0.01295	0.36	4.59		18.91
20	0 - 0.78	0.78	0.40	0.20095	0.00127	0.00099	0.00099	1.55	1.95	0.80005	1.432
	0.78 - 1.54	0.76	1.16	0.21407	0.00134	0.00102	0.00201	1.29	2.45		2.908
	1.54 - 2.31	0.77	1.91	0.21710	0.00139	0.00107	0.00308	1.06	2.97		4.456
	2.31 - 3.09	0.78	2.71	0.23356	0.00150	0.00117	0.00425	1.00	3.71		6.148
	3.09 - 3.85	0.76	3.47	0.23932	0.00112	0.00085	0.00510	0.80	4.27		7.358
	3.85 - 4.61	0.76	4.23	0.25580	0.00112	0.00085	0.00595	0.78	5.01		8.608
40	0 - 0.78	0.78	0.40	0.18409	0.00058	0.00045	0.00045	2.01	2.41	0.76146	0.6840
	0.78 - 1.54	0.76	1.16	0.19625	0.00062	0.00047	0.00092	1.70	2.86		1.398
	1.54 - 2.31	0.77	1.91	0.19962	0.00064	0.00049	0.00141	1.42	3.33		2.143
	2.31 - 3.09	0.78	2.71	0.21360	0.00069	0.00054	0.00195	1.36	4.07		2.964
	3.09 - 3.85	0.76	3.47	0.22427	0.00053	0.00040	0.00235	1.18	4.65		3.572
	3.85 - 4.61	0.76	4.23	0.23491	0.00053	0.00040	0.00275	1.05	5.28		4.180
80	0 - 0.78	0.78	0.40	0.16865	0.00027	0.00021	0.00021	2.61	3.01	0.69324	0.3509
	0.78 - 1.54	0.76	1.16	0.17988	0.00028	0.00021	0.00042	2.25	3.41		0.701
	1.54 - 2.31	0.77	1.91	0.18172	0.00029	0.00022	0.00064	1.89	3.80		1.069
	2.31 - 3.09	0.78	2.71	0.19535	0.00031	0.00024	0.00088	1.86	4.57		1.469
	3.09 - 3.85	0.76	3.47	0.21017	0.00025	0.00019	0.00107	1.74	5.21		1.786
	3.85 - 4.61	0.76	4.23	0.21846	0.00025	0.00019	0.00126	1.27	5.50		2.104
100	0 - 0.78	0.78	0.40	0.16396	0.00021	0.00016	0.00016	2.84	3.24	0.66618	0.2800
	0.78 - 1.54	0.76	1.16	0.17492	0.00022	0.00017	0.00033	2.46	3.62		0.5733
	1.54 - 2.31	0.77	1.91	0.17659	0.00023	0.00018	0.00051	2.07	3.98		0.8861
	2.31 - 3.09	0.78	2.71	0.18981	0.00024	0.00019	0.00070	2.05	4.76		1.216
	3.09 - 3.85	0.76	3.47	0.20583	0.00019	0.00014	0.00084	1.97	5.44		1.459
	3.85 - 4.61	0.76	4.23	0.21368	0.00019	0.00014	0.00098	1.34	5.57		1.703

TABLE 3

BEST FIT CURVES FOR
MATRIC POTENTIAL DATA

Depth (m)	Equation	r^2
0.40	$\psi = 0.506\ d^{0.374}$	0.93
1.16	$\psi = 0.392\ d^{0.398}$	0.96
1.91	$\psi = 0.308\ d^{0.414}$	0.97
2.71	$\psi = 0.264\ d^{0.445}$	0.95
3.47	$\psi = 0.147\ d^{0.656}$	0.97
4.23	$\psi = 0.050 + 0.285\ \ell n\ (d-7)$	0.99

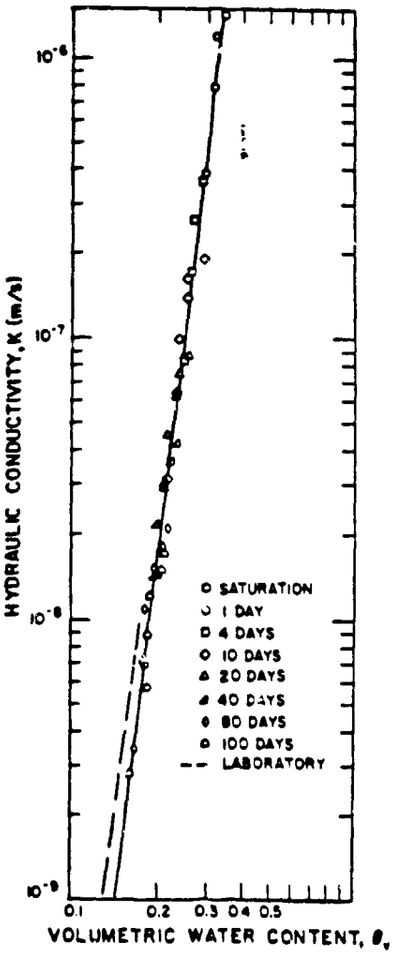

Fig. 9. Hydraulic conductivity as a function of volumetric water content calculated from the experimental results. The solid line is the best fit curve determined for all the measured values. The dashed curve is an extrapolation of the laboratory measurements.

CONSOLIDATION

When additional stress is applied to the saturated soil, the solid structure will not immediately support it because water will prevent compression (Fig. 10). Neutral stress supports the applied load. As the water is forced out, the soil compresses and the solid structure assumes more and more of the load until the neutral stress becomes zero and the solid particles support the total load or effective stress. The neutral stress can be read by means of a piezometer. Since pore water pressure measurements are not made in the oedometer, the degree of consolidation, U, is calculated directly from the change in height, H, of the sample, with U = 0% at the start of the consolidation and U = 100% at its completion. The change in void ratio $\Delta e = (1+e_o)\Delta H/H_o$. The time required to reach any percentage of consolidation for any thickness of a particular soil layer can be evaluated from the consolidation curve obtained in the laboratory. Any degree of consolidation to be obtained will be a function of the square of the thickness of a particular soil layer and its permeability at that particular consolidation pressure, so that rate and amount of settlement of a structure can be calculated. This would enable one to estimate whether settlements will be substantially completed during construction or how long they will last after completion. Means for accelerating the consolidation, such as sand drains or wicks, may be considered.

After equilibrium is reached and the transfer from neutral to effective stress is complete, the test proceeds by addition of a new load increment and allowing settlement to occur until equilibrium is reached under the new total stress, indicating the new consolidation is completed. For adequate computations of the coefficient of consolidation, C_v, standard load increments of $\Delta\sigma/\sigma$ equal to one must be used. A total final stress of one MPa was applied.

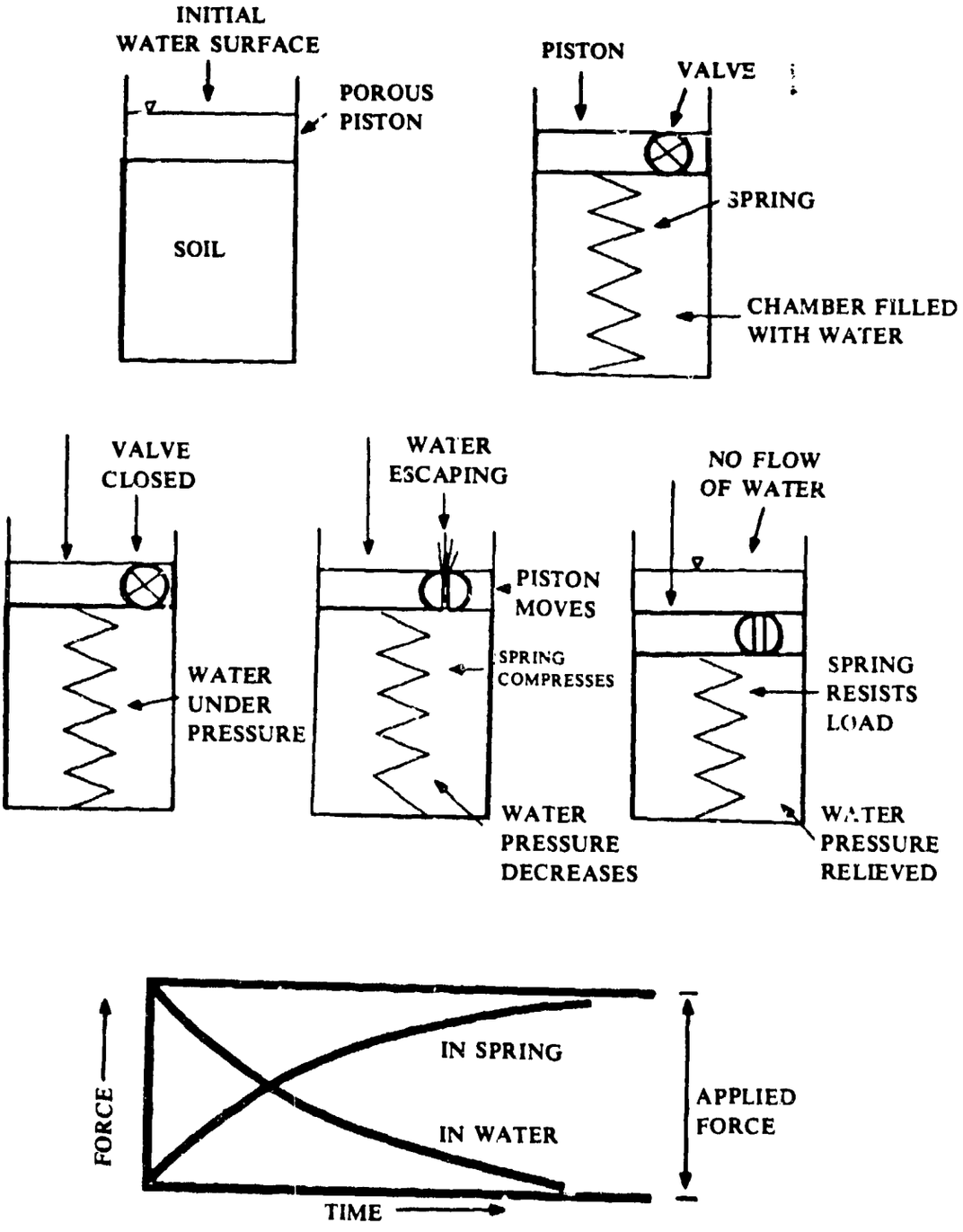

Fig. 10. Hydromechanical analogy for consolidation.

The compression characteristics of overconsolidated soil are demonstrated by the rebound (also: unloading, decompression, swelling) and recompression curve. If recompression is to take place, only above one MPa will a straight line equal to the existing one be obtained. The recompression curve indicates a soil that is overconsolidated and much less compressible than normally consolidated soils. The rebound is characteristic of the elastic deformation undergone by the soil, whereas the difference between original and rebound height is indicative of the plastic deformation undergone by the soil. Elastic deformation is reversible and is mainly caused by bending and distortion of the solid matrix, whereas reorientation and fracture of the solid particles account for plastic deformation.

Recompression curves are typically occurring in preconsolidated soils, which are soils once subjected to a stress exceeding the present overburden pressure. Removal of that overburden by erosion, melting, lowering of water table, or excavation leaves a soil preconsolidated. Most undisturbed soils are preconsolidated to some extent. This fact is extremely important in foundation engineering because such a soil will not appreciably settle until the stress imposed exceeds the preconsolidated stress.[7] An unconsolidated soil with a low C_v can be preloaded with fill if normal consolidation is expected to last until after completion of the structure.

The coefficient of consolidation increases naturally enough with increased permeability and decreased compressibility and is also inversely proportional to the specific weight of the diffusing fluid. Consequently, $k = C_v \lambda_w m_v$ ($m_v = d\epsilon/d\sigma$ with $\epsilon = \Delta H/H$).[8]

Crushed Bandelier tuff has a grain size distribution close to that of a silty sand. The specimen dimensions were 100 mm × 100 mm × 26 mm.

Mass of dry soil: 365 g.

Moisture ratio by mass: 0.323.

Particle density: 2.56 Mg m^{-3} (measured).

Initial void ratio: 0.323 × 2.56 = 0.83.

Porosity: 0.83/1.83 = 0.453.

Dry bulk density: 2.56/1.83 = 1.40 Mg m^{-3}.

Moisture ratio by volume: 0.323 × 1.40 = 0.45.

Saturated unit weight: (2.56+0.83)/1.83 = 1.85 Mg m^{-3}.

Volume: 365/1.40 = 260 cm^3.

Height of sample: 26 mm.

During consolidation, the data yielded void ratio/time curves concave upward from the start indicating extremely fast consolidation. The point t_{50}, indicating the time at which 50% of the consolidation is complete, was always passed before the first measurement could be taken (around 0.05 min). For our specimen of 26 mm thickness, C_v will then be at least 346 m^2/year or 1.1×10^{-5} $m^2 s^{-1}$.

The compression index C_c is the slope of the straight line where $e = -C_c \log \sigma/\sigma_o$. The compression index C_c is equal to 0.14635 above 60 kPa. The void ratio/stress curve is slightly convex upward. The swelling index S_c is equal to 0.01567 and 11% of the compression index of tuff.

The recompression curve follows a path almost identical to the rebound curve until the preconsolidation stress of one MPa is neared. Beyond one MPa, the recompression curve should merge with the virgin curve. The virgin, rebound, and recompression values at specific stresses are plotted in Fig. 11.

The best fit between hydraulic conductivity k and void ratio ϵ was determined through regression analysis: $k \propto 5.51 \times 10^{-13} e^{15.53\epsilon}$ with k expressed in m s^{-1} and $r = 0.97$. It is obvious that the values for the hydraulic conductivity are underestimated at all pressures because of an arbitrarily low choice of C_v.

At a porosity of 0.4 ($\epsilon = 0.67$), k would be equal to 1.81×10^{-8} m s^{-1}. Based on our field experiments, this is underestimating the measured hydraulic conductivity by a factor of close to 80. The relationship now becomes $k = 4.37 \times 10^{-11} e^{15.53\epsilon}$. A more correct C_v of 8.7×10^{-4} $m^2 s^{-1}$ can now be estimated from the intrinsic relationship between hydraulic conductivity and coefficient of consolidation. Because k was known, a more

direct approach could have been taken using Lambe's formula and computing C_v directly instead of trying to measure it. Our work also shows that only a static load of more than 250 kPa can match the void ratio obtained under dynamic loading in our field experiments, designed to measure hydraulic conductivity.

Current research at Los Alamos shows that crushed tuff mixed with upward of 8% bentonite clay has a coefficient of consolidation low enough so that it can easily be computed directly from the void ratio/log time graph.

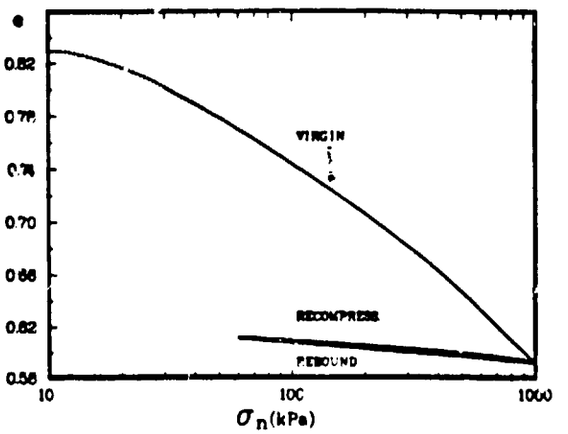

Fig. 11. Virgin, rebound, and recompression curves for crushed tuff.

CONSOLIDATED-DRAINED SHEAR TEST

Negative stress induced by capillary tension will be at the origin of increased soil shear strength. Capillary tension is the driving force that enables moist sand to maintain a molded or cut shape. Thin water films with small meniscus radii develop high-tensile stresses in the moisture wedges that hold soil particles in rigid contact. Fine sands and silts above a water table owe their strength to capillary tension and the resulting effective stresses in the granular structure. A point of maximum stress exists as a function of moisture content for a particular soil. In that case, any drying or wetting, away from that optimum moisture content, will mean a decrease in maximum shear strength. The components of shear strength are friction and cohesion. The friction component is primarily affected by mechanical factors, whereas physicochemical factors affect the cohesion component. Cohesion is dependent on attractive forces at work in clay particle interactions. Water plays an important role in determining the magnitude of the cohesion component because it affects the distance between soil particles and, consequently, the attractive forces associated with air/water menisci.[9] For any granular material, the strength characteristics depend heavily on the dry unit mass to which it is compacted. A higher dry unit mass will correspond to a higher shear strength, all other parameters being equal. Changes in dry unit mass and shear strength are both influenced by the same independent variable---moisture content. A plot of dry density vs moisture content will indicate that compaction at any given energy level becomes more efficient as the moisture content increases toward an optimum moisture level. Beyond this level, the efficiency decreases.

The least expensive way to improve soil stabilization is precisely through compaction. Soil stabilization, in turn, means the improvement of several physical properties, which, among other things, determine the shear strength of that soil. Besides an increase in shear strength, the other physical properties of a soil improved by compaction are the related increase in dry density and subsequent decreases in compressibility, permeability, and shrinkage (this last property is mainly applicable to montmorillonite). Adequate compaction of a pit overburden will improve several desirable properties important for good waste management.

A higher degree of consolidation means an increase in soil strength because of increased density. The consolidation process may continue during shearing (no increases in pore water pressure). The displacement rate during shearing is determined from the consolidation stage so that the potential further increase in consolidation is not hampered by the capacity to drain (a function of hydraulic conductivity).

If the sample is allowed to consolidate under the normal load before shearing and to drain during shearing, the test is termed a consolidated-drained (CD) test. Direct CD shear tests of the controlled strain type were performed at three or more different normal stresses for each different condition (preconsolidation level, moisture content). The three or more resulting stress/strain graphs obtained for the three or more applied normal stresses each yield a peak shear stress. The peak shear strengths are then plotted as a function of the effective normal stresses. The shear strength is then expressed analytically in the Coulomb equation

$$\tau = \sigma_{n_{eff}} \tan \phi + C.$$

Coulomb's equation shows that the shearing resistance is made up of two components:

- Friction, increasing with normal stress ($\sigma_{n_{eff}}$) is caused by the interlocking of particles. A good example of a frictional and cohensionless soil is sand. The Coulomb failure envelope passes through the origin.

- Cohesion, independent of normal stress. Coulomb's failure envelope is virtually horizontal if saturated clay is not allowed to consolidate before or drain during shearing.

For crushed tuff, no distinct peak was apparent. Practically no decrease in shear stress with increased displacement was noticed after attaining the ultimate shear stress (Figs. 12 through 15). Unpreconsolidated crushed tuff decreases in volume upon shearing, a behavior reminiscent of that of loose sand. That behavior changes if the sample is preconsolidated (Figs. 14 and 15), and dilatancy only occurs if the preconsolidated sample is sheared in a submerged shear-box (Fig. 15). Dry, unpreconsolidated crushed tuff has a shearing strength of $\tau = 12.43 + 0.775\ \sigma_n$; $r^2 = 0.99178$ (see Fig. 16).

For saturated, unpreconsolidated crushed tuff, moisture ratio by volume (MRV) = 0.453, and dry density (γ_d) = 1.40 Mg m^{-3}; $\tau = 8.72 + 0.73\ \sigma_n$; $r^2 = 0.99770$. For saturated crushed tuff, preconsolidated at one MPa, moisture ratio by volume (MRV) = 0.349 and dry unit weight (γ_d) = 1.667 Mg m^{-3}; $\tau = 23.48 + 0.819\ \sigma_n$; $r^2 = 0.99279$. For crushed tuff with a MRV = 0.30, γd = 1.610 Mg m^{-3} and preconsolidated at one MPa, $\tau = 23.74 + 0.719\ \sigma_n$; $r^2 = 0.99869$. The angle of repose, representing the angle of internal friction of a granular material at its loosest state, can be calculated from Coulomb's envelope. It amounts to 38° for crushed tuff. The repose angle of crushed tuff, which is higher than the normally expected range (30 to 35°), is probably mainly caused by a higher than average angularity, surface roughness, and grain size distribution, all of which will tend to increase the angle of repose.

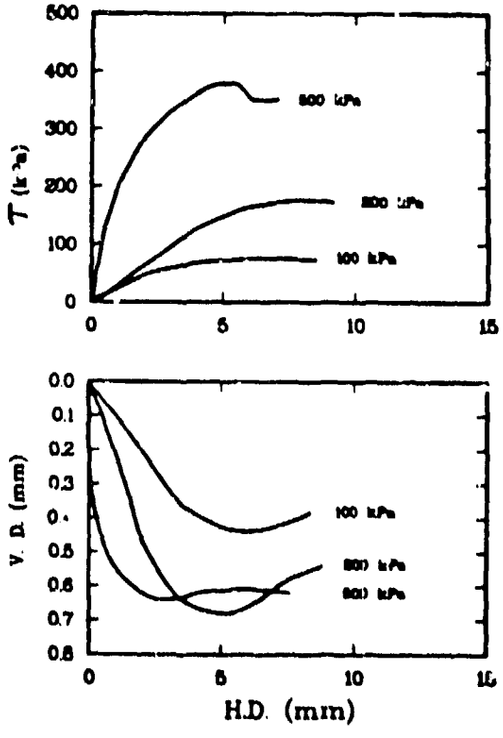

Fig. 12. Crushed tuff, no preconsolidation, MRV = 0.00.

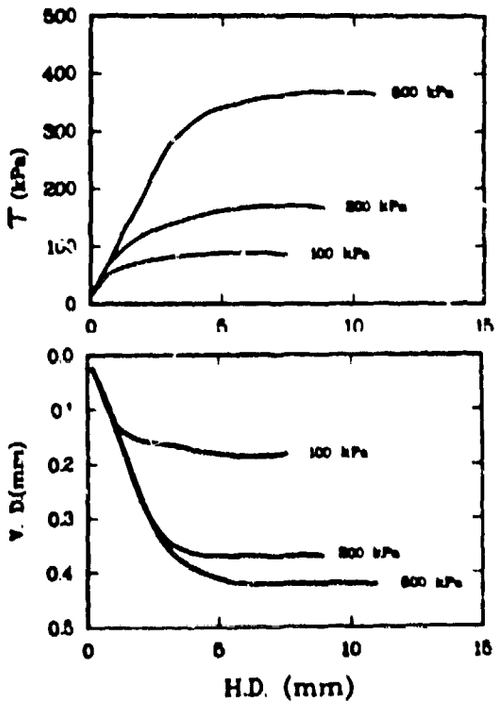

Fig. 13. Crushed tuff, no preconsolidation, MRV = 0.45.

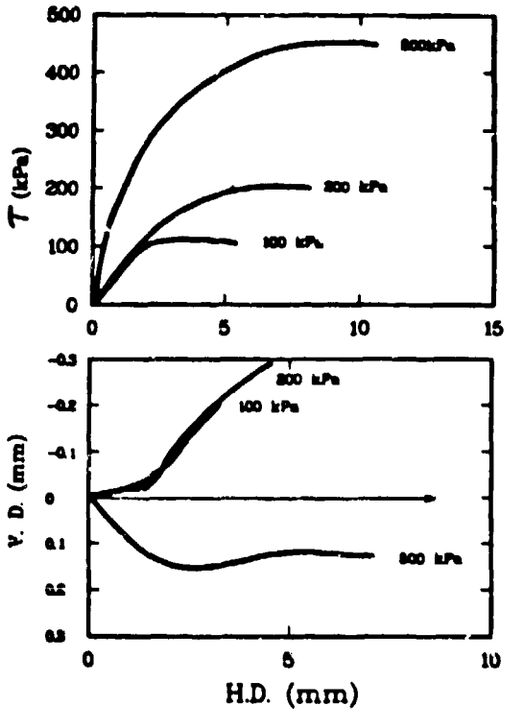

Fig. 14. Crushed tuff, preconsolidated at 1 MPa, MRV = 0.30.

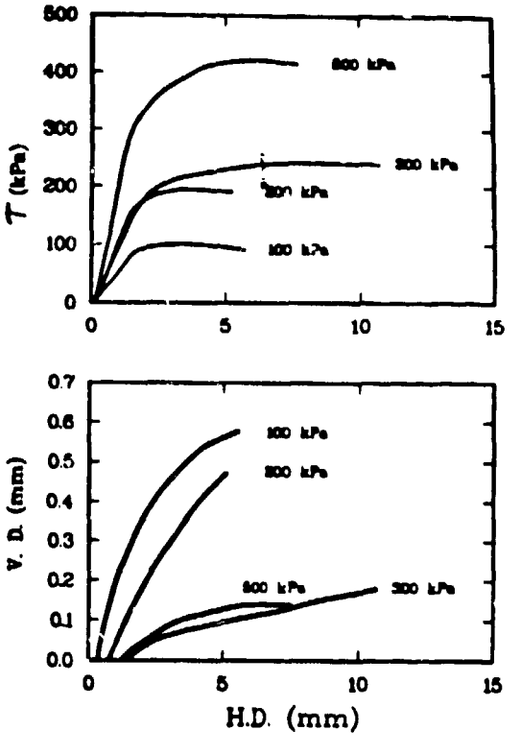

Fig. 15. Crushed tuff, preconsolidated at 1 MPa (submerged).

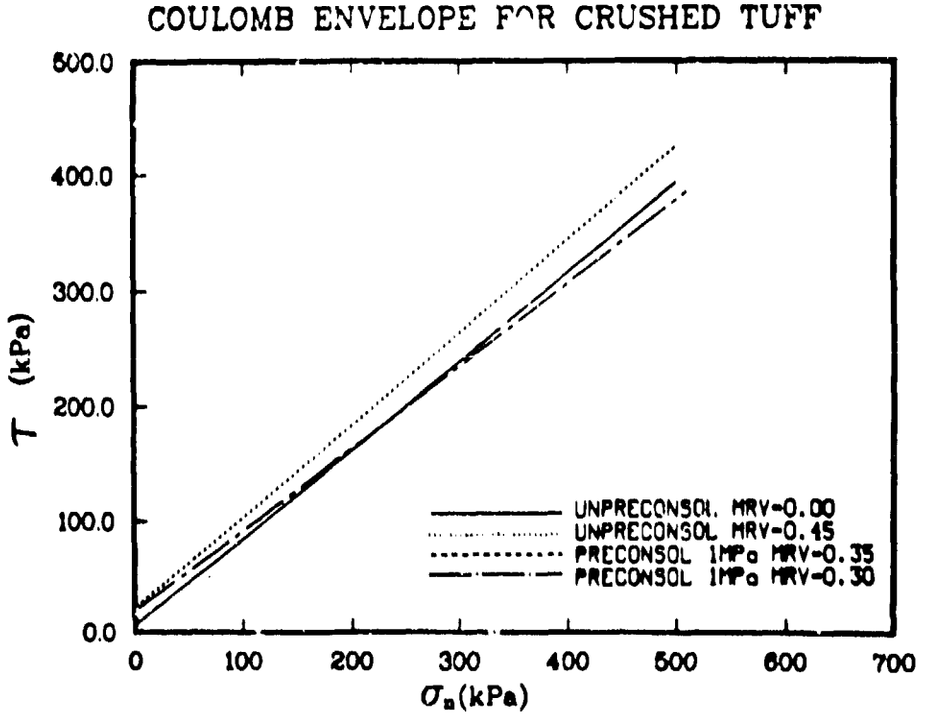

Fig. 16. Coulomb envelope for crushed tuff.

Knowledge of the shear strength of backfills is crucial in failure prediction of wick systems. Bond resistance to shear is currently under investigation for geotextile-based wick systems.

REFERENCES

1. Hakonson, T. E., G. C. White, and E. M. Karlen, "Evaluation of Geologic Materials to Limit Biological Intrusion of Low-Level Waste Covers," Proceedings ANS Topical Meeting on Treatment and Handling of Radioactives Wastes, April 19-22, 1982a, Richland, Washington.

2. Hakonson, T. E., J. R. Cline, and W. H. Rickard, "Biological Intrusion Barriers for Large Volume Waste Disposal Sites," in Proceedings Low-Level Waste Disposal: Facility Design, Construction and Operating Practices, NRC, September 29-30, 1982, Washington, DC.

3. Abeele, W. V., M. L. Wheeler, and B. W. Burton, "Geohydrology of Bandelier Tuff," Los Alamos National Laboratory report LA-8962-MS, October 1981.

4. Head, K. H., *Manual of Soil Laboratory Testing*, John Wiley & Sons, New York, 1981.

5. Nyhan, J. W. and B. J. Drennon, "Calibration and Field Testing of Three Neutron Moisture Gauges at Los Alamos," paper presented at the 1982 annual meeting of the American Society of Agronomy, Anaheim, California, November 1982.

6. Hillel, D., V. D. Krentos, and Y. Stylianou, "Procedure and Test of an Internal Drainage Method for Measuring Soil Hydraulic Characteristics *in situ*," 114(3), 395-400, 1972.

7. Abeele, W. V., "Determination of Hydraulic Conductivity in Crushed Bandelier Tuff," Los Alamos National Laboratory report LA-8147-MS, November 1979.

8. Watson, K. K., "An Instantaneous Profile Method for Determining the Hydraulic Conductivity of Unsaturated Porous Materials," Water Resources Research, 4(2), 709-714, 1966.

9. Sowers, G. F., *Soil Mechanics and Foundations: Geotechnical Engineering* 4th Ed., MacMillan Publishing Co., New York, 1979.

10. Lambe, T. W. and R. V. Whitman, *Soil Mechanics*, John Wiley & Sons, New York, 1979.

11. Baver, L. D., W. H. Gardner, and W. R. Gardner, *Soil Physics*, John Wiley & Sons, New York, 1972.